Advances in Applied Mathematics and Mechanics
Adv. Appl. Math. Mech., Vol. **4**, No. 3, pp. 294-310

DOI: 10.4208/aamm.10-m1167
June 2012

Simulation of Viscous Flows Around A Moving Airfoil by Field Velocity Method with Viscous Flux Correction

Ning Gu, Zhiliang Lu*and Tongqing Guo

Department of Aerodynamics, Nanjing University of Aeronautics and Astronautics, 29 Yudao Street, Nanjing 210016, China

Received 31 March 2011; Accepted (in revised version) 6 July 2011

Available online 30 April 2012

Abstract. Based on the field velocity method, a novel approach for simulating unsteady pitching and plunging motion of an airfoil is presented in this paper. Responses to pitching and plunging motions of the airfoil are simulated under different conditions. The obtained results are compared with those of moving grid method and good agreement is achieved. In the conventional field velocity method, the Euler solver is usually used to simulate the movement of the airfoil. However, when viscous effect is considered, unsteady Navier-Stokes equations have to be solved and the viscous flux correction must be taken into account. In this work, the viscous flux correction is introduced into the conventional field velocity method when non-uniform grid speed distribution is occurred. Numerical experiments for the flow around NACA0012 airfoil showed that the proposed approach can well simulate viscous moving boundary flow problems.

AMS subject classifications: 65Z05,65M04

Key words: Gust response, unsteady Navier-Stokes equations, field velocity method, viscous flux correction.

1 Introduction

In the field of Computational Fluid Dynamics (CFD), there are two categories of numerical methods for simulating moving boundary flow problems. One is the moving grid method [1–3], which constantly updates the grid according to the position of object. In this type of methods, the unsteady Navier-Stokes (N-S) equations are solved with the help of Arbitrary Lagrangian-Eulerian (ALE) technique. The major limitation of moving grid method is the regeneration of mesh at every time step, which may consume much time and reduce computational efficiency. To overcome this drawback, a

*Corresponding author.
Email: luzl@nuaa.edu.cn (Z. L. Lu)

pseudo grid-deformation approach was developed [4]. This approach calculates the grid speed through analytical expression of grid movement. The method is feasible to simulate rotational motion of the object. However, to simulate axial motion of the object, the volume change of grid cells should be considered. Another type of approaches for handling moving boundary problems is the field velocity method [5–8], which adopts the grid speed technique to simulate the velocity change of flow field. This method is especially suitable for calculation of step change of airfoil, and has been successfully applied to calculate the gust response of the airfoil/wing [9–12].

The conventional field velocity approach described above is usually used to calculate the indicial response [7, 8, 13]. It is a method for incorporating unsteady flow conditions via grid movement in CFD simulations. This approach provides a unique feature for directly calculating aerodynamic responses to step changes in flow conditions. Physically, the grid velocity can be interpreted as the velocity of a grid point in the mesh during the unsteady motion of the boundary surface. An impulsive change in the angle-of-attack can be perceived as an impulsive superposition of a uniform velocity field to the free stream. The magnitude of the normal velocity is determined by the magnitude of the indicial change for the angle-of-attack. This method effectively decouples the influence of pure angle-of-attack from that of a pitch rate because the airfoil is not made to pitch, and also because the step change is enforced over the entire flow domain uniformly. A similar methodology can be used for simulating responses of an airfoil to step changes in pitch rate and interaction with traveling vertical gusts or convecting vortices [13, 14]. In addition, the field velocity approach is also used to prescribe the effects of the trailed vortex wake from the other rotor blades [15–17], which reduces a lot of computational time as compared to the full wake capturing method. However, the observations from the time dependence study [15] strongly suggests that the consistent evaluation of time metrics for satisfying the geometric conservation law is critical for obtaining smooth and accurate solutions in time.

Based on the field velocity method, a novel technique is developed in this paper to simulate unsteady pitching and plunging motions of an airfoil by using a fixed grid. In the present work, the unsteady N-S equations are solved to describe the flow field. In the meanwhile, it is necessary to add a viscous flux correction to consider the gust responses when the grid speed is not uniform in space. In addition, to model the pitching motion, a rotational velocity is added to the grid to simulate the rotational speed of airfoil, and a vertical velocity to the grid to represent the angle change of airfoil. To model the plunging motion, only a vertical velocity is required. The present method is validated by its application to simulate the airfoil movement with different motion modes. The obtained results show good agreement with those of moving grid method. This demonstrates the capability of present field velocity method for simulation of moving boundary flow problems, and the ability to consider the gust response.

The paper is organized as follows. In Section 2, the viscous flux correction-based field velocity method is described in details. In Section 3, the proposed method is applied to simulate various moving airfoil problems to demonstrate its feasibility for

solving unsteady N-S equations. Some concluding remarks are given in Section 4.

2 Methodology

2.1 Governing equations and numerical discretization

To describe the flow field with moving airfoil, the unsteady N-S equations formulated in Cartesian coordinates are employed, which read [18]

$$\frac{\partial \overrightarrow{W}}{\partial t}+\frac{\partial \overrightarrow{f}}{\partial x}+\frac{\partial \overrightarrow{q}}{\partial z}=\Big(\frac{\partial \overrightarrow{R}}{\partial x}+\frac{\partial \overrightarrow{T}}{\partial z}\Big), \tag{2.1}$$

where $\overrightarrow{W}$ is the vector of conservative variables; $\overrightarrow{f}$ and $\overrightarrow{q}$ are the convective flux vectors in the x- and z-direction, respectively; $\overrightarrow{R}$ and $\overrightarrow{T}$ are the viscous flux vectors in x- and z-directions. The conservative variables are defined as follows

$$\overrightarrow{W}=\begin{bmatrix}\rho\\ \rho u\\ \rho w\\ \rho E\end{bmatrix}, \tag{2.2}$$

where ρ and E denote density and total energy per unit mass respectively, and u, w are the velocity components in Cartesian coordinates. The convective flux vectors and the viscous flux vectors are defined as follows

$$\overrightarrow{f}=\begin{bmatrix}\rho U\\ \rho U u+p\\ \rho U w\\ (\rho E+p)U+x_t p\end{bmatrix}, \qquad \overrightarrow{q}=\begin{bmatrix}\rho W\\ \rho W u\\ \rho W w+p\\ (\rho E+p)W+z_t p\end{bmatrix}, \tag{2.3a}$$

$$\overrightarrow{R}=\begin{bmatrix}0\\ \tau_{xx}\\ \tau_{zx}\\ u\tau_{xx}+w\tau_{xz}+k\dfrac{\partial T}{\partial x}\end{bmatrix}, \qquad \overrightarrow{T}=\begin{bmatrix}0\\ \tau_{xz}\\ \tau_{zz}\\ u\tau_{zx}+w\tau_{zz}+k\dfrac{\partial T}{\partial z},\end{bmatrix}, \tag{2.3b}$$

where p is the static pressure of the fluid and T is the static temperature, $U=u-x_t$, $W=w-z_t$. Here, x_t and z_t denote the velocity components of grid speed $\vec{v}_t$ in Cartesian coordinates. The notation τ_{ij} means the stress component in a plane perpendicular to the i-axis in the direction of the j-axis.

The spatial discretization of N-S equations is performed using the Jameson central scheme with artificial dissipation. The dual time-stepping approach [19] is adopted for time integration. The Spalart-Allmaras (S-A) one equation model [20] is employed to simulate the turbulent flow. A uniform flow field is taken as the initial condition, and the non-slip and non-reflecting boundary conditions are applied on the wall and far-field boundary, respectively [21]. In this work, the C-type structured grid is used for numerical computation. For the rest of this subsection, the descriptions of Jameson scheme and S-A turbulence model are presented.

First, the Jameson scheme is depicted simply. Consider a control volume Ω with boundary $\partial\Omega$ which moves with flow velocity. The governing equations can be written in the integral form as [18]

$$\frac{\partial}{\partial t}\int_{\Omega}\overrightarrow{W}d\Omega+\oint_{\partial\Omega}(\overrightarrow{F}_c-\overrightarrow{F}_v)dS=0, \tag{2.4}$$

where $\overrightarrow{F}_c$ is the vector of convective fluxes, $\overrightarrow{F}_v$ is the vector of viscous fluxes, and dS is the surface element of Ω.

The convective flux through a face of the control volume is approximated using the average of variables. Artificial dissipation is then added to the central fluxes for stability. The total convective flux at face $(I+1/2,J)$ reads

$$(\overrightarrow{F}_c\Delta S)_{I+\frac{1}{2},J}\approx\overrightarrow{F}_c(\overrightarrow{W}_{I+\frac{1}{2},J})\Delta S_{I+\frac{1}{2},J}-\overrightarrow{D}_{I+\frac{1}{2},J}, \tag{2.5}$$

where I, J denote the index of a control volume, ΔS is the area of one face of the control volume. The flow variables are averaged as

$$\overrightarrow{W}_{I+\frac{1}{2},J}=\frac{1}{2}(\overrightarrow{W}_{I,J}+\overrightarrow{W}_{I+1,J}). \tag{2.6}$$

For simplicity, $(I+1/2,J)$ will be abbreviated as $(I+1/2)$ hereafter. The artificial dissipation flux consists of a blend of adaptive second- and fourth-order differences which result from the sum of first- and third-order difference operators

$$\overrightarrow{D}_{I+\frac{1}{2}}=\hat{\Lambda}^S_{I+\frac{1}{2}}\left[\varepsilon^{(2)}_{I+\frac{1}{2}}(\overrightarrow{W}_{I+1}+\overrightarrow{W}_I)-\varepsilon^{(4)}_{I+\frac{1}{2}}(\overrightarrow{W}_{I+2}-3\overrightarrow{W}_{I+1}+\overrightarrow{W}_I-\overrightarrow{W}_{I-1})\right], \tag{2.7}$$

where $\varepsilon^{(2)}$ and $\varepsilon^{(4)}$ are parameters of the pressure-based sensor. The dissipation is scaled by the sum of the spectral radii of the convective flux Jacobian in all coordinate directions

$$\hat{\Lambda}^S_{I+\frac{1}{2}}=(\hat{\Lambda}^I_c)_{I+\frac{1}{2}}+(\hat{\Lambda}^J_c)_{I+\frac{1}{2}}+(\hat{\Lambda}^K_c)_{I+\frac{1}{2}}. \tag{2.8}$$

The spectral radius at the cell face $(I+1/2)$ is evaluated from the average

$$(\hat{\Lambda}^I_c)_{I+\frac{1}{2}}=\frac{1}{2}\big((\hat{\Lambda}^I_c)_I+(\hat{\Lambda}^I_c)_{I+1}\big), \tag{2.9}$$

$\hat{\Lambda}_c$ can be computed by

$$(\hat{\Lambda}^I_c)=(|V|+c)\Delta S, \tag{2.10}$$

where V stands for the contravariant velocity and c is the speed of sound.

After spatial discretization, a system of coupled ordinary differential equations in time can be obtained as

$$\frac{d}{dt}(\Omega_I\overrightarrow{W}_I)+\overrightarrow{R}_I(\overrightarrow{W})=0, \tag{2.11}$$

where $\overrightarrow{R}$ represents the residual. In order to obtain a fully-implicit algorithm, Eq. (2.11) can be written as

$$\frac{d}{dt}(\Omega_I^{n+1}\overrightarrow{W}_I^{n+1}) + \overrightarrow{R}_I(\overrightarrow{W}^{n+1}) = 0, \tag{2.12}$$

where the superscript $n+1$ denotes the time level $(n+1)\Delta t$. The time derivative in Eq. (2.12) can be approximated by the following second order implicit scheme,

$$\frac{d(\Omega_I^{n+1}\overrightarrow{W}_I^{n+1})}{dt} = \frac{3\Omega_I^{n+1}\overrightarrow{W}_I^{n+1} - 4\Omega_I^{n}\overrightarrow{W}_I^{n} + \Omega_I^{n-1}\overrightarrow{W}_I^{n-1}}{2\Delta t}. \tag{2.13}$$

As a result, Eq. (2.12) can be approximated as

$$\frac{3\Omega_I^{n+1}\overrightarrow{W}_I^{n+1} - 4\Omega_I^{n}\overrightarrow{W}_I^{n} + \Omega_I^{n-1}\overrightarrow{W}_I^{n-1}}{2\Delta t} + \overrightarrow{R}_I(\overrightarrow{W}^{n+1}) = 0. \tag{2.14}$$

Equation system (2.14) is a set of algebraic equations. By setting

$$\overrightarrow{W}^{*} = \overrightarrow{W}^{n+1}, \tag{2.15a}$$

$$\overrightarrow{R}_I^{*}(\overrightarrow{W}^{*}) = \overrightarrow{R}_I(\overrightarrow{W}^{*}) + \frac{3}{2\Delta t}\Omega_I^{n+1}\overrightarrow{W}_I^{*} - \frac{2}{\Delta t}\Omega_I^{n}\overrightarrow{W}_I^{n} + \frac{1}{2\Delta t}\Omega_I^{n-1}\overrightarrow{W}_I^{n-1}, \tag{2.15b}$$

and with introduction of a pseudo-time derivative $\partial\overrightarrow{W}_I^{*}/\partial\tau$, Eq. (2.14) can be written as

$$\frac{\partial\overrightarrow{W}_I^{*}}{\partial\tau} + \overrightarrow{R}_I^{*}(\overrightarrow{W}^{*}) = 0. \tag{2.16}$$

Within each real time step, equation system (2.16) can be solved using a five-stage Runge-Kutta scheme.

After the description of Jameson scheme, the Spalart-Allmaras one equation turbulence model is presented as follows. The integral form of S-A turbulence model over a control volume can be written as [20]

$$\frac{\partial}{\partial t}\int_\Omega \tilde{v}d\Omega + \oint_{\partial\Omega}(F_{c,T} - F_{v,T})dS = \int_\Omega Q_T d\Omega, \tag{2.17}$$

where d denotes the distance to the closest wall, $\tilde{v}$ is the eddy-viscosity. The convective flux is defined as

$$F_{c,T} = \tilde{v}V, \tag{2.18}$$

with V being the contravariant velocity. The convective flux is in general discretized using the first-order upwind scheme. The viscous flux is given by

$$F_{v,T} = n_x\tau_{xx}^T + n_y\tau_{yy}^T + n_z\tau_{zz}^T, \tag{2.19}$$

where n_x, n_y, n_z are the components of the unit normal vector. The viscous stresses can be expressed by

$$\tau_{xx}^T = \frac{1}{\sigma}(v_L + \tilde{v})\frac{\partial \tilde{v}}{\partial x}, \qquad \tau_{yy}^T = \frac{1}{\sigma}(v_L + \tilde{v})\frac{\partial \tilde{v}}{\partial y}, \qquad \tau_{zz}^T = \frac{1}{\sigma}(v_L + \tilde{v})\frac{\partial \tilde{v}}{\partial z}. \tag{2.20}$$

Here, v_L denotes the laminar kinematic viscosity. The source term in Eq. (2.17) is given by

$$Q_T = C_{b1}(1 - f_{t2})\widetilde{\Omega}\tilde{v} + \frac{C_{b2}}{\sigma}(\nabla\tilde{v})^2 - \Big(C_{w1}f_w - \frac{C_{b1}}{\kappa^2}f_{t2}\Big)\Big(\frac{\tilde{v}}{d}\Big)^2 + f_{t1}\|\Delta\vec{v}\|_2^2, \tag{2.21a}$$

$$\widetilde{\Omega} = \Omega + \frac{\tilde{v}}{\kappa^2 d^2}f_{v2}, \quad f_{v2} = 1 - \frac{\chi}{1 + \chi f_{v1}}, \quad f_{v1} = \frac{\chi^3}{\chi^3 + C_{v1}^3}, \quad \chi = \frac{\tilde{v}}{v_L}, \tag{2.21b}$$

where Ω stands for the magnitude of the mean rotational rate. The parameters used in Eq. (2.21) are computed by

$$f_w = g\Big(\frac{1 + C_{w3}^6}{g^6 + C_{w3}^6}\Big)^{\frac{1}{6}}, \qquad g = r + C_{w2}(r^6 - r), \quad r = \frac{\tilde{v}}{\widetilde{\Omega}\kappa^2 d^2}, \tag{2.22a}$$

$$f_{t1} = C_{t1}g_t \exp\Big[-C_{t2}\frac{\Omega_t^2}{\|\Delta\vec{v}\|_2^2}(d^2 + g_t^2 d_t^2)\Big], \quad f_{t2} = C_{t3}\exp(C_{t4}\chi^2), \quad g_t = \min\Big[0.1, \frac{\|\Delta\vec{v}\|_2}{(\Omega_t \Delta x_t)}\Big], \tag{2.22b}$$

where Ω is the vorticity on the wall at the trip point, $\|\Delta\vec{v}\|_2$ denotes the L2-norm of the difference between the velocity at the trip point and the current field point, d_t is the distance to the nearest trip point, and Δx_t stands for the spacing along the wall at the trip point. The coefficients used in above equations are taken as

$$C_{b1} = 0.1355, \quad C_{b2} = 0.622, \quad C_{v1} = 7.1, \quad C_{v2} = 5, \tag{2.23a}$$

$$\sigma = \frac{2}{3}, \quad \kappa = 0.41, \quad C_{w1} = \frac{C_{b1}}{\kappa^2} + \frac{1 + C_{b2}}{\sigma}, \quad C_{w2} = 0.3, \tag{2.23b}$$

$$C_{w3} = 2.0, \quad C_{t1} = 1, \quad C_{t2} = 2, \quad C_{t3} = 1.3, \quad C_{t4} = 0.5. \tag{2.23c}$$

After spatial discretization, Eq. (2.17) can also be solved using the five-stage Runge-Kutta scheme.

2.2 Moving grid method

In this section, the moving grid method is simply described first as this method will be used to verify our proposed field velocity method with viscous correction. Here, an elastic moving grid method is adopted, in which the grid of wall boundary is firstly generated, and then an elastic mesh deformation technique is utilized to generate the grid of internal flow field [22].

The coordinates (represented by subscript u) of the dynamic grid are [23]

$$x_u = x_r - (x_r - x_s)\cdot g, \tag{2.24}$$

where subscript s represents the boundary-fitted static grid which is used as the initial grid; r represents the instantaneous grid which is changed from the static grid; g is the function about the serial number of the grid lines.

To validate the moving grid method, a NACA0012 airfoil is forced to pitch around the quarter chord with a reduced frequency of 0.0814. The form of pitching motion is given as follows

$$\alpha = 0.016^0 + 2.51^0 \sin \omega t, \tag{2.25}$$

where α is the angle of attack, ω is the reduced frequency, t is the time. The Reynolds number Re, based on the chord of airfoil, is 5.5×10^6, and the Mach number Ma is 0.755. In this case, the unsteady Euler/N-S equations are solved. The results calculated by Euler equations are compared with the reference data calculated by Deng et al. [1] and the experimental data as depicted in Fig. 1. As shown in this figure, the results of moving grid method basically compare well with the data in the literature. The differences may be attributed to the mesh quality and the pseudo-time error. Fig. 2 shows the results calculated by N-S equations and those of Jahangirian and Hadidoolab [2]. The slight differences in minus angle in Fig. 2 are due to the selection of pseudo-time, steady-state error as mentionedin [2]. From two figures, it can be seen that the current results are in good agreement with both the experimental data and the reference result. This demonstrates the feasibility of moving grid technique used in this paper.

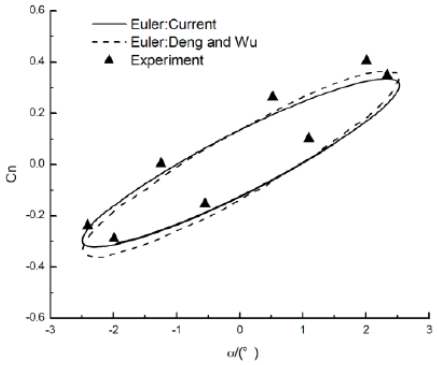

Figure 1: Calculated normal force by solving Euler equations.

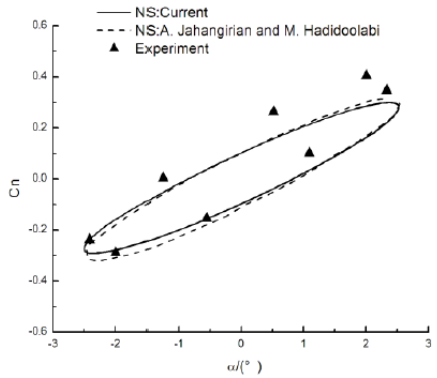

Figure 2: Calculated normal force by solving N-S equations.

2.3 Field velocity method

Conventionally, the velocity vector $\overrightarrow{V}$ in the field velocity approach can be written as [7,8]

$$\overrightarrow{V} = (u - x_t)\vec{i} + (w - z_t)\vec{k}, \tag{2.26}$$

where u and w are the velocity components along x- and z- direction; x_t and z_t are the grid speed components along x- and z- directions, respectively. Since the indicial step change in the angle can be represented by the velocity along z- direction, Eq. (2.26) can be written as

$$\overrightarrow{V} = (u - x_t)\vec{i} + (w - z_t + w_g)\vec{k}. \tag{2.27}$$

Eq. (2.27) provides a way to determine the response resulting from a pure step change in the angle of attack without any dependent pitch rate term. To validate this field velocity method, the response of a NACA0012 airfoil under indicial gust is simulated. The grid speed w_g is set as

$$w_g(\hat{\tau}) = w_0 U_{step}(\hat{\tau}), \tag{2.28}$$

where $\hat{\tau}$ is the non-dimensional time, $U_{step}(\hat{\tau})$ is the unit step function and w_0 is the amplitude of the step function. The gust velocity amplitude is 0.08 times of the upstream flow velocity. The calculations are performed at $Ma = 0.3$, 0.5 and 0.8. Fig. 3 plots the lift responses of airfoil. Also shown in Fig. 3 is the reference result of [8]. Fig. 4 compares the lift responses calculated by Euler and N-S solvers. As shown in Fig. 3, the current lift responses agree well with those in [8]. The results in Fig. 4 show that the gust responses calculated by N-S equations are qualitatively close to those from Euler equations. This shows that the field velocity method can be well incorporated into the N-S and Euler solvers.

Based on the conventional field velocity method, a new approach for handling unsteady pitching and plunging motion of airfoil on a fixed grid is presented. In this method, to simulate the pitching motion, the treatment of indicial change in angle and

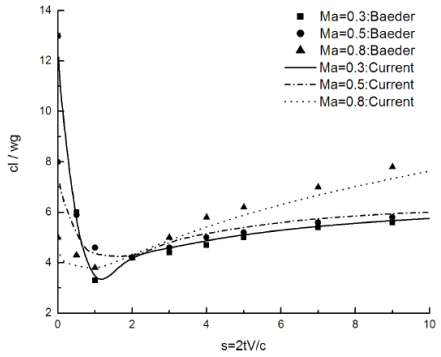

Figure 3: Comparison of lift response with [8] by Euler solver.

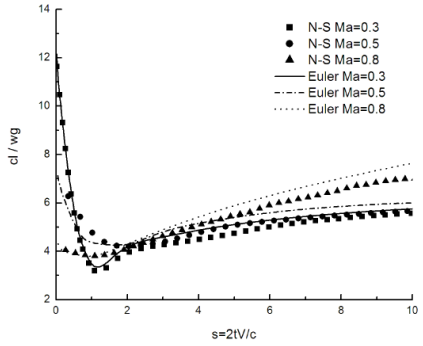

Figure 4: Comparison of calculated lift response by Euler and N-S solvers.

angular velocity is decoupled. The indicial change in angle is regarded as a velocity in z- direction as shown in Eq. (2.27), while the indicial change in angular velocity is considered by adding a rotating velocity. The resultant formulation is

$$\overrightarrow{V} = (u - x_t + |y|w_x)\vec{i} + (w - z_t + |x|w_y)\vec{k}, \tag{2.29}$$

where x and y denote the location of the grid relative to the rotational axis; w_x and w_y denote the components of angular velocity along coordinate directions. The grid speed in Eq. (2.29) is added to account for the effect of angular speed of fluid, which is the indicial change in angular velocity. By solving Eqs. (2.27) and (2.29), the unsteady pitching motion of airfoil can be calculated without moving the grid. As compared to pitching motion, it is very easy to deal with plunging motion in the present method. Only the vertical grid speed is added to represent the plunging motion.

2.4 Viscous flux correction

According to the principle of relative motion, which is shown in Fig. 5, the downward speed of grid V' is equivalent to the upward speed of cell center V'. In the moving grid system, the vector of viscous fluxes is only related to the speed of the viscous fluxes is also related to the speed of the fluid, which should be changed because of the relative motion of the fluid V' in Fig. 5, and its effect on the viscous force as well as the work done by the viscous force and pressure should be considered. For a grid cell, the velocity which is used to calculate the viscous flux must be the vector summation of initial velocity V and grid velocity V'. When the field velocity method is directly applied to solve the unsteady N-S equations (2.1), the grid velocity is not considered. Therefore, the conventional field velocity method can not accurately simulate the practical flow phenomena. This is because the viscous flux due to non-zero grid speed is not included in the simulation.

As for the convective flux, the grid speed V' has been taken into account when the flux is calculated across the face of cells. Therefore, solving Euler equations with the help of field velocity method could accurately deal with moving airfoil problems. When solving N-S equations, however, the viscous flux must be corrected at every

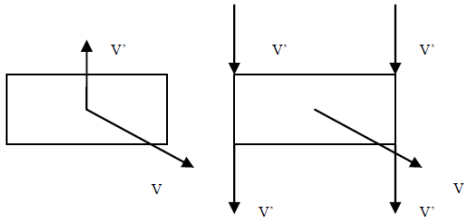

Figure 5: Comparison of moving grid method and field velocity method.

time-step. This means that the effect of the grid speed which contributes to the viscous flux should be considered. Hence, the following correction is adopted at the beginning of every time-step

$$\rho = \rho_0, \quad \rho u = \rho_0(u_0 - u_{gc}), \quad \rho w = \rho_0(w_0 - w_{gc}), \quad \rho E = \rho_0 E_0, \tag{2.30}$$

where the subscript 0 denotes the physical values of cell center at previous time-step, u_{gc} and w_{gc} denote the transformed grid speed of cell center along x- and z- direction, respectively.

The stresses caused by the grid speed can be written as follows

$$\tau_{xx} = 2\mu\frac{\partial u_{gc}}{\partial x} - \frac{2}{3}\mu\Big(\frac{\partial u_{gc}}{\partial x} + \frac{\partial u_{gc}}{\partial z}\Big), \tag{2.31a}$$

$$\tau_{xz} = \tau_{zx} = \mu\Big(\frac{\partial u_{gc}}{\partial z} + \frac{\partial u_{gc}}{\partial x}\Big), \tag{2.31b}$$

$$\tau_{zz} = 2\mu\frac{\partial u_{gc}}{\partial z} - \frac{2}{3}\mu\Big(\frac{\partial u_{gc}}{\partial x} + \frac{\partial u_{gc}}{\partial z}\Big), \tag{2.31c}$$

where μ is the dynamic viscosity. If the grid speed is uniform in space, we have

$$\frac{\partial w_g}{\partial x} = 0, \qquad \frac{\partial w_g}{\partial z} = 0, \qquad \frac{\partial u_g}{\partial x} = 0, \qquad \frac{\partial u_g}{\partial z} = 0, \tag{2.32}$$

where u_g and w_g stand for the grid speed of the cell vertex in Cartesian coordinates.

The viscous stresses in Eq. (2.31) are zero in this situation, which means that the grid speed does not contribute to the viscous flux. So the viscous flux correction is not required. On the other hand, it should be stressed that the heat conduction terms $k\partial T/\partial x$ and $k\partial T/\partial z$ do change due to different velocities of cell centre, but the resultant effect is not obvious, which is studied in test case 3.2. If the grid speed is not uniform in space, the viscous flux correction is required due to non-zero viscous stresses on the right-hand side of Eq. (2.1).

3 Three types of grid speed and numerical verification

In this work, the forms of grid speed considered can be classified into three types.

3.1 Type 1: pitching motion

In this situation, the form of grid speed has the following feature

$$\frac{\partial w_g}{\partial x} \neq 0, \qquad \frac{\partial w_g}{\partial z} \neq 0, \qquad \frac{\partial u_g}{\partial x} = 0, \qquad \frac{\partial u_g}{\partial z} \neq 0. \tag{3.1}$$

Generally, the viscous flux caused by the grid speed is not zero. The grid speed is given for the pitching motion as

$$\frac{\partial w_g}{\partial x} = \pm w_r, \qquad \frac{\partial w_g}{\partial z} = 0, \qquad \frac{\partial u_g}{\partial x} = 0, \qquad \frac{\partial u_g}{\partial z} = \pm w_r, \tag{3.2}$$

where w_r is the angular velocity. As the first test case, the flow around the NACA0012 airfoil at $Ma = 0.755$ is considered. It is forced to pitch around the quarter chord at a reduced frequency of 0.0814. The form of the motion is

$$\alpha = 0.016^0 + 2.51^0 \sin \omega t. \tag{3.3}$$

The unsteady Euler equations are solved first, and the results calculated by the field velocity method without viscous correction and the moving grid method are compared in Fig. 6. It is clear from the figure that the result calculated by the field velocity method without viscous correction is in good agreement with that from the moving grid method. This implies that the field velocity method produces little numerical errors by solving unsteady Euler equations.

Next, the same problem is simulated by solving unsteady N-S equations. The calculated results via field velocity method with and without viscous correction and moving grid method are compared in Fig. 7. For this case, the result of field velocity method without viscous correction cannot compare well with that of moving grid method. The discrepancy is attributed to the fact that the viscous flux due to grid speed is not considered. After introduction of viscous flux correction, the obtained result can agree very well with the data from the moving grid method.

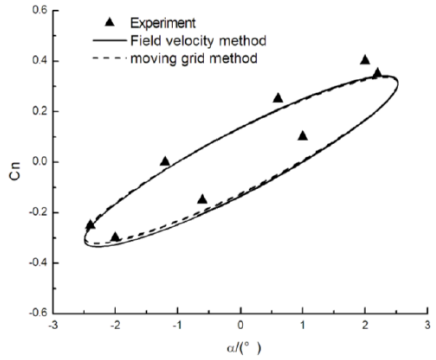

Figure 6: Comparison of normal force by Euler solver.

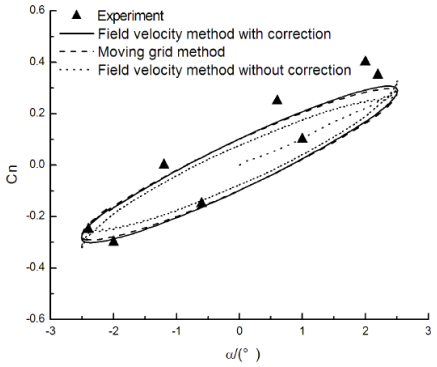

Figure 7: Comparison of normal force by N-S solver.

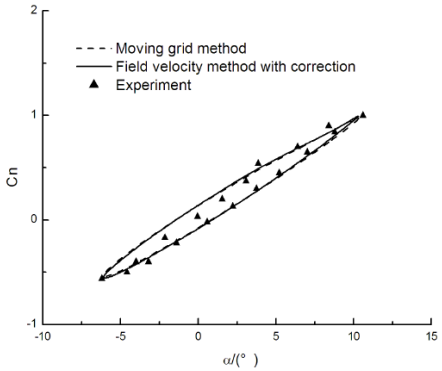

Figure 8: Comparison of normal force by N-S solver in large angle.

As the second test case, the NACA0012 airfoil performs the pitching motion at a reduced frequency of 0.074 with $Ma = 0.383$. The form of the motion is

$$\alpha = 2.1^\circ + 8.2^\circ \sin \omega t. \tag{3.4}$$

Here, the unsteady N-S equations are solved. The comparisons between the results calculated by the field velocity method with viscous flux correction, the moving grid method and the experimental data are shown in Fig. 8. Good agreement in the figure shows that the field velocity method with viscous correction is a suitable tool for the simulation of attached flow at relatively high angles of attack. From Figs. 7 and 8, the conclusion can be made that the viscous correction is indispensable to accurately calculate the viscous flux when the grid speed is not uniform in space.

3.2 Type 2: indicial and sharp-edged gusts, plunging

In this situation, the grid speed is uniform in the whole flow field. Thus, the form of grid speed is

$$\frac{\partial w_g}{\partial x} = 0, \qquad \frac{\partial w_g}{\partial z} = 0, \qquad \frac{\partial u_g}{\partial x} = 0, \qquad \frac{\partial u_g}{\partial z} = 0. \tag{3.5}$$

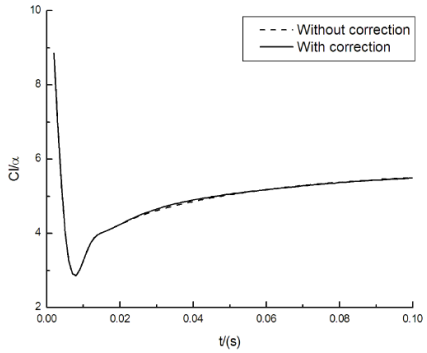

Figure 9: Calculated lift response of indicial gust by N-S solver.

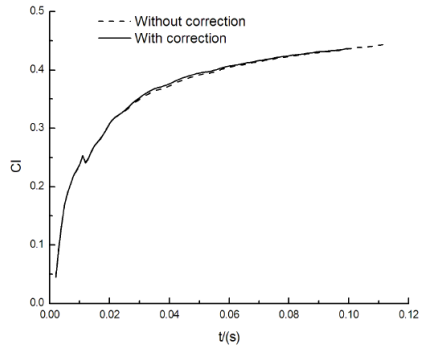

Figure 10: Calculated lift response of sharp-edged gust by N-S solver.

Since the viscous flux caused by grid speed is zero, the viscous flux correction is unnecessary. To verify the method, the NACA0012 airfoil is supposed to encounter the indicial and sharp-edged gusts. For numerical simulation, Ma is taken as 0.3 and the gust amplitude is 0.08 times of upstream velocity. The results calculated by unsteady N-S equations with and without viscous flux correction are shown in Figs. 9 and 10. It can be seen from the figures that the curves of lift evolution for two cases are nearly the same, which means that the viscous flux correction has little influence on the results.

As the second test case for this type of grid speed, the NACA0012 airfoil is forced to plunge at a reduced frequency of 0.8 with $Ma = 0.3$. The form of the motion is

$$h = 0.2 \sin \omega t, \tag{3.6}$$

where h is the non-dimensional plunge distance of airfoil. Again, the unsteady N-S equations are solved. The results calculated by the field velocity method with and without viscous correction as well as the moving grid method are compared in Fig. 11. It is obvious from the figure that the viscous flux correction has little effect on the result of this type of grid speed.

On the other hand, it should be pointed out that the differences in Figs. 9-11 are caused by the fact that the terms $k\partial T/\partial x$ and $k\partial T/\partial z$ do change due to the effect of correction. Nevertheless, it can be found that the differences are obviously very small.

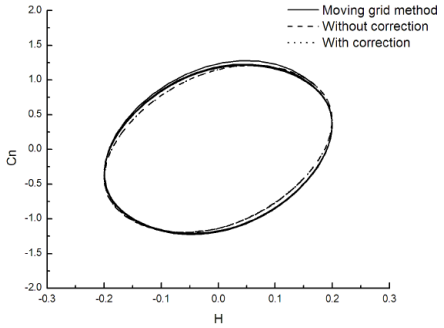

Figure 11: Calculated normal force for plunging by N-S solver.

Therefore, it can be concluded that the viscous flux correction is unnecessary when the grid speed is uniform in the whole flow field.

3.3 Type 3: vertical 1-cosine and sine gust

In this situation, the form of grid speed is given as

$$\frac{\partial w_g}{\partial x} \neq 0, \qquad \frac{\partial w_g}{\partial z} = 0, \qquad \frac{\partial u_g}{\partial x} = 0, \qquad \frac{\partial u_g}{\partial z} = 0. \tag{3.7}$$

There is a velocity gradient of vertical grid speed in the x- direction for this case. As a result, the viscous flux caused by the grid speed is not zero. At the same time, the airfoil enters the gust area gradually.

As the first test case for this type of grid speed, the NACA0012 airfoil executes discrete 1-cosine gust with $Ma = 0.3$. The gust shape is defined as follows

$$w_g = \frac{1}{2} w_0 \Big[1 - \cos\Big(\frac{2\pi x}{h} \Big) \Big], \tag{3.8}$$

where $w_0 = 0.05$ and $h = 5.0$. The results calculated by unsteady N-S equations with and without viscous flux correction are compared in Fig. 12. From the figure, we can see that the influence of viscous flux correction is not very obvious for this case.

Next, the case of sine gust with $Ma = 0.3$ is considered. The gust shape is defined as follows

$$w_g = -\frac{1}{2} w_0 \sin\Big(\frac{2\pi x}{h} \Big), \tag{3.9}$$

where $w_0 = 0.05$ and $h = 5.0$. The results calculated by unsteady N-S equations with and without viscous flux corrections based on different meshes are compared in Fig. 13. The calculations for the airfoil are performed on the coarse C-type mesh with 225 points in the wrap around direction, 49 points in the normal direction, and on the fine mesh with 241 points in the wrap around direction, 111 points in the normal direction. For the case with viscous flux correction, the lift evolutions remain the same by using coarse and fine grids. In the situation without viscous flux correction, the

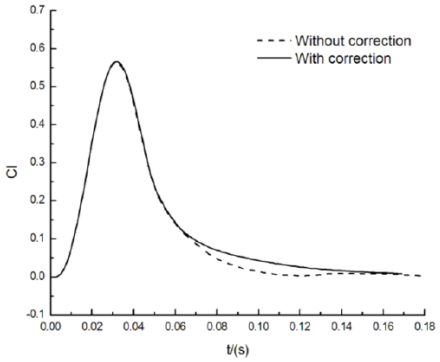

Figure 12: Calculated lift response of 1-cosine gust by N-S solver.

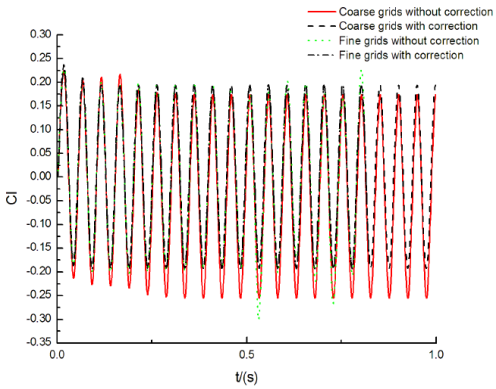

Figure 13: Calculated lift response of sin gust by N-S solver.

amplitude of the lift variation with respect to time becomes larger on the coarse grid, which is probably induced by accumulation of errors due to less accurate calculation of viscous fluxes. To improve the solution, the fine grids have to be used. After some time steps, however, the amplitude still fluctuates irregularly. From Figs. 12 and 13, it can be seen that the viscous correction is still required to obtain the accurate computation of viscous flux. However, since the airfoil enters the gust area gradually, the effect of non-uniform grid speed on numerical results is not obvious, which is similar to the case in Section 3.1. This may demonstrate that the viscous flux correction is imperative for this case.

4 Conclusions

Based on the viscous flux correction, a new field velocity method for computing the unsteady pitching and plunging motions of airfoil on a fixed grid is developed in this paper. As for the pitching motion, a rotational velocity is added to the grid to simulate the rotational speed of airfoil, and a vertical velocity to the grid to represent the angle change of airfoil. As for the plunging motion, only a vertical velocity is required. The method is able to simulate the movement of the airfoil, and the regeneration of

mesh at every time step is not needed, which reduces computational time greatly. Numerical experiments showed that when the unsteady N-S equations are solved with non-uniform grid speed, an example being the simulation of 1-cosine, sine gust and pitching motion, the viscous correction must be added when calculating the viscous flux.

Through the obtained numerical results, the proposed approach is proven to be accurate when solving unsteady N-S equations. As compared to the moving grid method which usually consumes much time, it has a potential to be widely used to simulate various moving boundary flow problems. In addition, the present method can also provide a basic tool when applied to the simulation of the gust response.

Acknowledgments

This work was supported by The National Basic Research Program of China (Grant No. 2007CB714600) and Funding of Jiangsu Innovation Program for Graduate Education (Grant No. CXLX11_0170).

References

[1] F. DENG, Y. Z. WU AND X. Q. LIU, *Numerical simulation of two-dimensional unsteady viscous flow based on hybrid dynamic grids*, Journal of Nanjing University of Aeronautics & Astronautics, 39 (2009), pp. 444–448.
[2] A. JAHANGIRIAN AND M. HADIDOOLABI, *Unstructured moving grids for implicit calculation of unsteady compressible viscous flows*, Int. J. Numer. Meth. Fluids., 47 (2005), pp. 1107–1113.
[3] C. FARHAT, C. DEGAND, B. KOOBUS AND M. LESOINNE, *An improved method of spring analogy for dynamic unstructured fluid meshes*, AIAA., 98-2070.
[4] H. TADGHIGHI, Z. LIU AND S. V. RAMAKRISHNAN, *A pseudo grid-deformation approach for simulation of unsteady flow past a helicopter in hover and forward flights*, AIAA, 05-1361.
[5] H. ZHAN AND W. Q. QIAN, *Numerical simulation of gust response for airfoil and wing*, Acta. Aerodyn. Sinica., 25 (2007), pp. 532–536.
[6] H. ZHAN AND W. Q. QIAN, *Numerical simulation on gust response of elastic wing*, Chinese J. Comput. Mech., 26 (2009), pp. 271–275.
[7] R. SINGH AND J. D. BAEDER, *Direct calculation of three dimensional indicial lift response using computational fluid dynamics*, J. Aircraft., 34 (1997), pp. 465–471.
[8] V. PARAMESWARAN AND J. D. BAEDER, *Indicial aerodynamics in compressible flow-direct computational fluid dynamic calculation*, J. Aircraft., 34 (1997), pp. 131–133.
[9] H. GOPALAN AND A. POVITSKY, *A numerical study of gust suppression by flapping airfoils*, AIAA., 08-6394.
[10] G. W. YANG, *Numerical analyses of discrete gust response for an aircraft*, J. Aircraft., 41 (2004), pp. 1353–1359.
[11] D. E. RAVEH, *CFD-based models of aerodynamic gust response*, AIAA., 06-2022.
[12] D. E. RAVEH, *CFD-based gust response analysis of free elastic aircraft*, AIAA., 09-2539.
[13] J. SITARAMAN AND J. D. BADER, *Enhanced unsteady airload models using CFD*, AIAA., 00-33847.

[14] R. SINGH AND J. D. BAEDER, *On the significance of transonic effects on aerodynamics and acoustics of blade vortex interaction*, AIAA., 96-1697.
[15] J. SITARAMAN AND J. D. BAEDER, *Field velocity approach and geometric conservation law for unsteady flow simulations*, AIAA. J., 44 (2006), pp. 2084–2094.
[16] J. SITARAMAN, J. D. BAEDER AND I. CHOPRA, Validation of UH-60A Blade Aerodynamic Characteristics Using CFD, Proceedings of the 59th Annual Forum of American Helicopter Society, 2003.
[17] J. SITARAMAN, A. DATTA, I. CHOPRA AND I. J. BAEDER, Coupled CFD/CSD Prediction of Rotor Aerodynamic and Structural Dynamic Loads for Three Critical Flight Conditions, Proceedings of the 31st European Rotorcraft Forum, 2005.
[18] J. BLAZEK, Computational Fluid Dynamics: Principles And Applications, Kidlington: Elsevier Science Ltd: 5-22, 2001.
[19] A. JAMESON, W. SCHMIDT AND E. TURKEL, *Numerical solution of the Euler equations by finite volume methods using Runge-Kutta time-stepping scheme*, AIAA., 81-1259.
[20] S. R. SPALART AND S. A. ALLMARAS, *A one-equation turbulence model for aerodynamic flows*, AIAA., 92-0439.
[21] K. MAZAHERI AND P. L. ROE, *Numerical wave propagation and steady-state solutions: soft wall and outer boundary conditions*, AIAA. J., 35 (1997), pp. 965–975.
[22] T. Q. GUO, Transonic Unsteady Aerodynamics and Flutter Computations for Complex Assemblies, Ph. D. Thesis, Nanjing University of Aeronautics and Astronautics, 2006.
[23] Z. L. LU, *Generation of dynamic grids and computation of unsteady transonic flows around assemblies*, Chinese Journal of Aeronautics, 2001.